


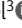
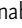

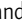


BRIEF DEFINITIVE REPORT

Sensing of endogenous nucleic acids by ZBP1 induces keratinocyte necroptosis and skin inflammation

Michael Devos^{1,2*} , Giel Tanghe^{1,2*} , Barbara Gilbert^{1,2}, Evelien Dierick^{1,2}, Maud Verheirstraeten^{1,2}, Josephine Nemegeer^{1,2}, Richard de Reuver^{1,2}, Sylvie Lefebvre^{1,2}, Jolien De Munck^{1,2} , Jan Rehwinkel³ , Peter Vandenebeele^{1,2} , Wim Declercq^{1,2**} , and Jonathan Maelfait^{1,2**} 

Aberrant detection of endogenous nucleic acids by the immune system can cause inflammatory disease. The scaffold function of the signaling kinase RIPK1 limits spontaneous activation of the nucleic acid sensor ZBP1. Consequently, loss of RIPK1 in keratinocytes induces ZBP1-dependent necroptosis and skin inflammation. Whether nucleic acid sensing is required to activate ZBP1 in RIPK1-deficient conditions and which immune pathways are associated with skin disease remained open questions. Using knock-in mice with disrupted ZBP1 nucleic acid-binding activity, we report that sensing of endogenous nucleic acids by ZBP1 is critical in driving skin pathology characterized by antiviral and IL-17 immune responses. Inducing ZBP1 expression by interferons triggers necroptosis in RIPK1-deficient keratinocytes, and epidermis-specific deletion of MLKL prevents disease, demonstrating that cell-intrinsic events cause inflammation. These findings indicate that dysregulated sensing of endogenous nucleic acid by ZBP1 can drive inflammation and may contribute to the pathogenesis of IL-17-driven inflammatory skin conditions such as psoriasis.

Introduction

Erroneous detection of endogenous nucleic acids by pattern recognition receptors (PRRs) of the innate immune system can cause the development of inflammatory diseases. This phenomenon is best described in the context of a group of human autoinflammatory and autoimmune disorders, termed type I interferonopathies (Crowl et al., 2017; Lee-Kirsch, 2017; Rodero and Crow, 2016). Gain-of-function mutations in genes encoding components of the nucleic acid sensing pathways, including *TMEM173* (stimulator of interferon genes [STING]) and *IFIH1* (MDA5), result in enhanced detection of endogenous nucleic acids (Jeremiah et al., 2014; Liu et al., 2014; Rice et al., 2014). Conversely, loss-of-function of genes controlling nucleic acid metabolism such as *TREX1*, *SAMHD1*, and *ADAR* result in the reduced clearance of endogenous nucleic acids and trigger spontaneous production of type I IFNs, which initiate and sustain inflammatory disease development (Crow et al., 2006; Rice et al., 2009, 2012).

The nucleic acid receptor Z-DNA binding protein 1 (ZBP1) restricts RNA and DNA virus infection by mechanisms including the induction of regulated necroptotic cell death (Kuriakose and Kanneganti, 2018). Although regulated cell

death is a vital antiviral defense strategy, excessive cell death is thought to contribute to the pathogenesis of inflammatory diseases (Newton and Manning, 2016; Pasparakis and Vandenebeele, 2015; Weinlich et al., 2017). Execution of necroptosis results in cell membrane rupture and the release of intracellular components including damage-associated molecular patterns, which activate innate immune receptors, thereby initiating a detrimental inflammatory response. The release of antigens by dying cells may promote adaptive immune responses, further driving autoimmune pathology and establishing chronic disease (Galluzzi et al., 2017).

In mouse cells, the induction of necroptosis following ZBP1 engagement occurs via the direct recruitment of the serine/threonine protein kinase RIPK3 through RIP homotypic interaction motifs (RHIMs), which are present in both RIPK3 and ZBP1 (Upton et al., 2012). RIPK3 then phosphorylates mixed lineage kinase domain-like pseudokinase (MLKL) on serine 345, leading to its oligomerization and translocation to the plasma membrane, where it damages the integrity of the cell membrane (Wallach et al., 2016). In contrast to necroptosis triggered by TNF, necroptosis downstream of ZBP1 does not require the

¹VIB Center for Inflammation Research, Ghent, Belgium; ²Department of Biomedical Molecular Biology, Ghent University, Ghent, Belgium; ³Medical Research Council Human Immunology Unit, Medical Research Council Weatherall Institute of Molecular Medicine, Radcliffe Department of Medicine, University of Oxford, Oxford, UK.

*M. Devos and G. Tanghe contributed equally to this paper; **W. Declercq and J. Maelfait contributed equally to this paper; Correspondence to Jonathan Maelfait: jonathan.maelfait@irc.vib-ugent.be; Wim Declercq: wim.declercq@irc.vib-ugent.be; J. De Munck's present address is Department of Pharmaceutical Biotechnology and Molecular Biology, Vrije Universiteit Brussel, Brussels, Belgium.

© 2020 Devos et al. This article is distributed under the terms of an Attribution-Noncommercial-Share Alike-No Mirror Sites license for the first six months after the publication date (see <http://www.rupress.org/terms/>). After six months it is available under a Creative Commons License (Attribution-Noncommercial-Share Alike 4.0 International license, as described at <https://creativecommons.org/licenses/by-nc-sa/4.0/>).

kinase activity of the RHIM-containing signaling kinase RIPK1 (Upton et al., 2012). In keratinocytes, RIPK1 ablation or disruptive mutation of the RHIM of RIPK1 induces spontaneous ZBP1-dependent necroptosis and triggers skin inflammation, indicating that RIPK1 acts as a molecular scaffold to inhibit ZBP1-RIPK3-MLKL signaling in a RHIM-dependent way (Dannappel et al., 2014; Lin et al., 2016; Newton et al., 2016).

ZBP1 contains two tandem N-terminal Z-form nucleic acid binding ($Z\alpha$)-domains, which specifically interact with double-stranded (ds) nucleic acid helices in the Z-conformation, including Z-RNA and Z-DNA (Herbert, 2019). Others and our group have shown that engagement of ZBP1 upon virus infection crucially depended on nucleic acid sensing by intact $Z\alpha$ -domains (Maelfait et al., 2017; Sridharan et al., 2017; Thapa et al., 2016). The identity of viral ZBP1 agonists remains uncertain, and viral ribonucleoprotein complexes, RNA genomes, or viral transcripts have been suggested to interact with the $Z\alpha$ -domains of ZBP1 (Guo et al., 2018; Kesavardhana et al., 2017; Maelfait et al., 2017; Sridharan et al., 2017; Thapa et al., 2016; Zhang et al., 2020). The importance of Z-form nucleic acid interaction with ZBP1 during viral infection raises the question whether endogenous nucleic acids can also stimulate ZBP1 when certain checkpoints such as RIPK1 are compromised and whether aberrant nucleic acid sensing by ZBP1 could provoke the development of inflammatory disease.

To address this question, we crossed epidermis-specific RIPK1-deficient mice, which developed inflammatory skin disease, to *Zbp1* knock-in animals with mutated $Z\alpha$ -domains, rendering ZBP1 unable to interact with Z-form nucleic acids (Maelfait et al., 2017). Using this genetic approach, we show that skin pathology critically depends on nucleic acid sensing by ZBP1. The epidermis of keratinocyte-specific RIPK1-deficient mice displayed enhanced expression of antiviral genes, including *Zbp1*, and is characterized by infiltration of IL-17-producing CD4 T cells and innate lymphoid cells (ILCs). Finally, in vitro type I (IFN β) or type II IFN (IFN γ) treatment of RIPK1-deficient keratinocytes induced necroptosis, while RIPK1-deficient cells expressing $Z\alpha$ -domain mutant ZBP1 were protected. Together, these data suggest that endogenous nucleic acid sensing by ZBP1 triggers cell-intrinsic necroptosis of RIPK1-deficient keratinocytes, which initiates an inflammatory signaling cascade causing skin pathology.

Results and discussion

Skin pathology of *Ripk1*^{EKO} mice is dependent on nucleic acid sensing by ZBP1

Mice with epidermis-specific deletion of RIPK1 develop progressive ZBP1-dependent skin inflammation (Dannappel et al., 2014; Lin et al., 2016). To determine if nucleic acid sensing by ZBP1 is required for skin pathology, we crossed *Ripk1*^{FL/FL} K5Cre^{Tg/+} animals (*Ripk1*^{EKO}; Ramirez et al., 2004; Takahashi et al., 2014) to mice carrying a *Zbp1* allele (*Zbp1*^{Z α 1 α 2}) mutated in the two $Z\alpha$ -domain coding regions, resulting in the expression of a ZBP1 protein that is unable to interact with its nucleic acid agonist. We have previously shown that *Zbp1*^{Z α 1 α 2/Z α 1 α 2} mice are susceptible to a strain of murine cytomegalovirus that does

not block necroptosis downstream of ZBP1 (Maelfait et al., 2017). *Ripk1*^{EKO} mice developed skin pathology with macroscopically visible lesions starting 1 wk after birth (Fig. 1 A and Fig. S1 A). In contrast, *Ripk1*^{EKO} *Zbp1*^{Z α 1 α 2/Z α 1 α 2} animals remained lesion-free until at least 12 wk after birth (Fig. 1 A), whereupon more than half of the mice displayed smaller and more focal lesions compared with *Ripk1*^{EKO} littermates, and these lesions did not develop further until 1 yr of age. One intact allele of *Zbp1* was sufficient to initiate disease development, albeit with delayed kinetics (Fig. 1 A). ZBP1 protein levels were not affected by $Z\alpha$ -domain mutation or the absence of RIPK1 in primary keratinocytes treated with IFN β to induce the expression of ZBP1 (Fig. S1 B). Importantly, the interaction between ZBP1 and RIPK3 was not disrupted due to $Z\alpha$ -domain mutation as RIPK3 coimmunoprecipitated equally efficient with wild-type and mutant ZBP1 (Fig. S1 C). Absence of inflammation was confirmed by histological examination of skin of 4–5-wk-old *Ripk1*^{EKO} *Zbp1*^{Z α 1 α 2/Z α 1 α 2} mice, as shown by normal epidermal thickness (Fig. 1, B and C) and a normal expression pattern of the epidermal differentiation markers keratin-1, -5 and -6, compared with *Ripk1*^{EKO} mice (Fig. 1 B). As previously described, *Ripk1*^{EKO} mice crossed to full-body *Zbp1* knock-out animals displayed a similarly rescued phenotype as the *Ripk1*^{EKO} *Zbp1*^{Z α 1 α 2/Z α 1 α 2} line (Fig. S1 D; Lin et al., 2016). Deletion of *Ripk3* or reducing its gene dosage by half was sufficient to establish substantial protection, confirming that activation of RIPK3 led to skin pathology (Fig. S1 E; Dannappel et al., 2014). Loss of RIPK3 offered better protection against lesion formation than ZBP1 $Z\alpha$ -domain mutation or deficiency, indicating that other RHIM-containing signaling complexes, most likely mediated by TRIF (TIR domain containing adaptor inducing IFN β), contribute to disease progression (Dannappel et al., 2014). We conclude that intact $Z\alpha$ -domains are crucial for ZBP1-induced lesion formation in *Ripk1*^{EKO} mice, indicating that nucleic acid sensing by ZBP1 drives keratinocyte necroptosis in the absence of RIPK1.

ZBP1 activation drives an IL-17 immune response in *Ripk1*^{EKO} mice

Next, we determined the presence of immune cells in inflammatory lesions of *Ripk1*^{EKO} mice by flow cytometry (Fig. S2 A). The total number of CD45⁺ leukocytes was significantly increased in *Ripk1*^{EKO} epidermis, and this was dependent on nucleic acid sensing by ZBP1 (Fig. 2 A and Fig. S2 A). In healthy mouse skin, $\gamma\delta$ -TCR⁺ dendritic epidermal T cells constitute the majority of leukocytes (Nielsen et al., 2017); however, their numbers did not significantly increase in RIPK1-deficient skin (Fig. 2 A and Fig. S2 A). In contrast, RIPK1-deficient epidermis displayed a marked infiltration of $\alpha\beta$ -TCR⁺ CD4 T cells, which reached similar levels as dendritic epidermal T cells. The accumulation of CD4 T cells depended on intact nucleic acid sensing by ZBP1 as these cells were reduced to wild-type levels in the epidermis of *Ripk1*^{EKO} *Zbp1*^{Z α 1 α 2/Z α 1 α 2} mice (Fig. 2 A and Fig. S2 A). Further quantification showed a ZBP1-dependent influx of CD8 T cells, natural killer T cells, neutrophils, and CD64⁺ myeloid cells (Fig. 2 A and Fig. S2 A). In vitro activation assays on cells isolated from the epidermis of *Ripk1*^{EKO} mice revealed that the majority of the CD4 T cells produced the cytokine IL-17A, but not

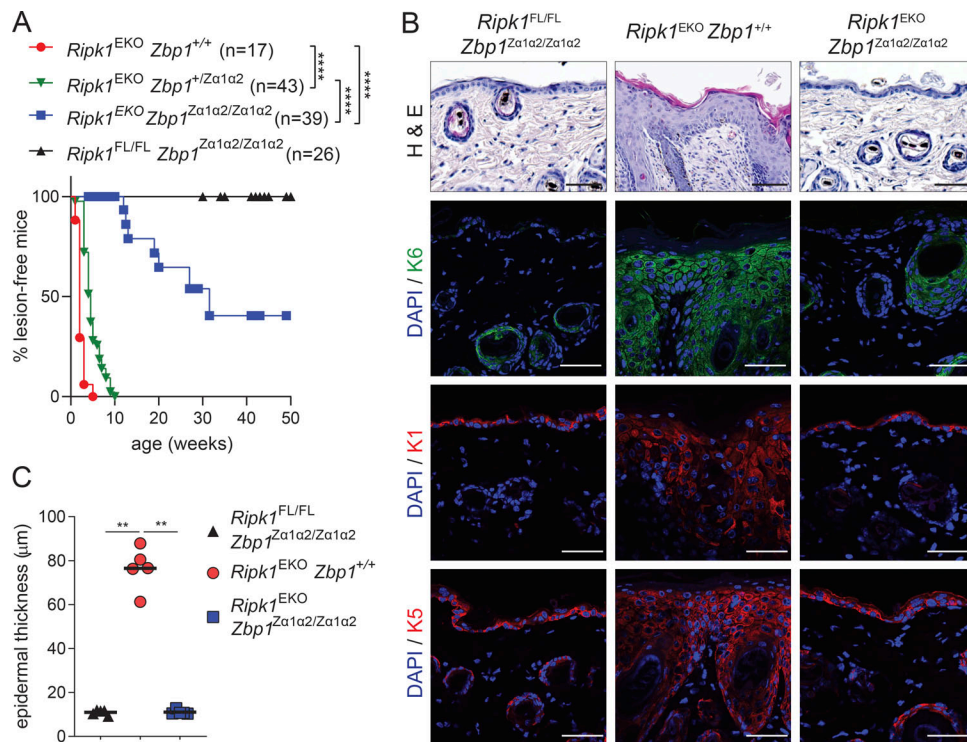


Figure 1. Skin pathology of *Ripk1^{EKO}* mice is dependent on nucleic acid sensing by ZBP1. (A) Kaplan–Meier plot of macroscopically visible lesion appearance of epidermis-specific RIPK1-deficient mice (*Ripk1^{EKO}*), *Ripk1^{EKO}* mice carrying heterozygous (*Zbp1^{+/Za1a2}*) or homozygous (*Zbp1^{Za1a2/Za1a2}*) *Zbp1* *Za*-domain mutant alleles. Littermates that did not express the keratinocyte-specific K5-Cre transgene (*Ripk1^{FL/FL} Zbp1^{Za1a2/Za1a2}*) were used as controls. Pictures of lesions are shown in Fig. S1A. ****, $P < 0.0001$ by log-rank test. **(B)** Back skin sections of 4–5-wk-old mice with indicated genotypes were stained with H&E or immunostained for keratin-6 (K6), keratin-1 (K1), or keratin-5 (K5) antibodies and DAPI. Scale bars, 50 μm . At least four mice per genotype were analyzed. **(C)** Quantification of epidermal thickness on H&E-stained sections shown in B. The line represents the mean, and dots represent individual mice. **, $P < 0.01$ by Mann–Whitney *U* test. Data are representative of at least two independent experiments.

IFN γ , identifying these cells as helper T (Th) 17 cells (Fig. 2, B and C). A large fraction of the CD45⁺ leukocytes stained negative for many of the cell surface markers used in our staining panel; however, they produced large amounts of IL-17A and equaled Th17 cells in total cell numbers (Fig. 2, B and C). We concluded that these cells most likely represent type 3 ILCs (ILC3s). At 5 wk of age, the infiltration of IL-17A–producing CD4 T cells and ILC3s was not observed in *Ripk1^{EKO} Zbp1^{Za1a2/Za1a2}* mice. However, the epidermis of 10–12-wk-old *Ripk1^{EKO} Zbp1^{Za1a2/Za1a2}* animals contained increased numbers of Th17 and ILC3s (Fig. 2 C), which coincided with the development of mild skin pathology and correlated with the incomplete phenotypic rescue of these mice (see Fig. 1 A). In addition, we detected ZBP1-dependent increased messenger RNA expression of the IL-17A regulatory cytokine IL-23 in RIPK1-deficient epidermis (Fig. 2 D). Together, these results indicate that in the absence of RIPK1, the detection of nucleic acids by ZBP1 triggers keratinocyte necroptosis, which induces an IL-17-mediated inflammatory response.

Induction of MLKL-dependent necroptosis by ZBP1 in keratinocytes drives skin inflammation in *Ripk1^{EKO}* mice

ZBP1 expression is inducible by type I and type II IFNs, and its expression is increased in RIPK1-deficient epidermis (Lin et al., 2016). We therefore examined whether skin lesions of *Ripk1^{EKO}* mice showed a general antiviral gene signature. Indeed, messenger

RNA expression of a panel of IFN-stimulated genes (ISGs; *Zbp1*, *Ifi44*, *Isg15*, and *Ifit1*) and type II IFN (*Ifng*) was enhanced in 5-wk-old *Ripk1^{EKO}* mice, and this was fully restored in a ZBP1 *Za*-domain mutant background (Fig. 3 A and Fig. S2 B). In addition, increased expression of inflammatory cytokines (*Il6*, *Il1b*, *Il1a*, *Il33*), the chemokine *Ccl20*, and antimicrobial peptide *S100a8* required intact *Za*-domains of ZBP1 (Fig. 3 A and Fig. S2 B). To determine in which cell types ZBP1 was expressed in inflamed *Ripk1^{EKO}* skin, we performed immunostaining of ZBP1. In normal skin, ZBP1 expression is restricted to a few dermal cells, probably myeloid cells such as macrophages, which express high basal levels of ZBP1 (Lin et al., 2016; Newton et al., 2016). In contrast, inflamed epidermis from *Ripk1^{EKO}* mice displayed strong cytosolic staining for ZBP1 in keratinocytes (Fig. 3 B), consistent with the enhanced ZBP1 messenger RNA expression in these lesions (Fig. 3 A). The high expression of ZBP1 in RIPK1-deficient keratinocytes could induce MLKL-dependent necroptosis in these cells to drive skin inflammation in *Ripk1^{EKO}* mice. To test this hypothesis, we crossed *Ripk1^{EKO}* mice to *Mlkl^{FL/FL}* animals (Murphy et al., 2013), generating mice lacking both RIPK1 and MLKL in keratinocytes. Similar to complete ZBP1 deficiency, ablating MLKL specifically in keratinocytes profoundly attenuated the development of lesion formation (Fig. 3 C). In addition to inducing necroptosis, ZBP1 engagement has been reported to activate the NLRP3 inflammasome, leading to caspase-1-dependent pyroptosis and IL-1 β release (Kuriakose

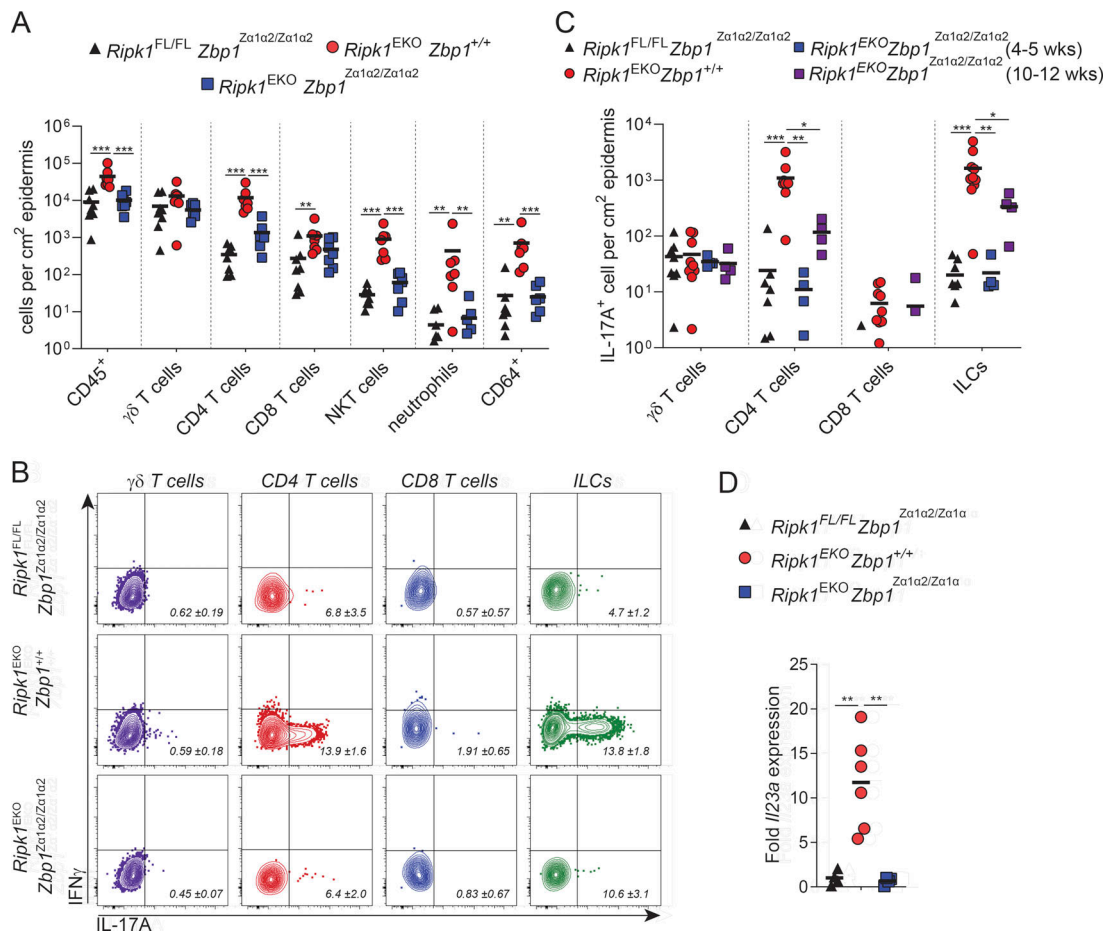


Figure 2. ZBP1 activation drives an IL-17 immune response in *Ripk1*^{EKO} mice. (A) Flow cytometry analysis of leukocyte (CD45⁺) composition of epidermis of mice of the indicated genotypes. The number of immune cells per square centimeter of epidermis is plotted. Each dot represents an individual mouse, and the line represents the mean. The gating strategy is outlined in Fig. S2 B. **(B and C)** Epidermal cells isolated from 4–5-wk-old *Ripk1*^{FL/FL} *Zbp1*^{Za1a2/Za1a2}, *Ripk1*^{EKO} *Zbp1*^{+/+}, or *Ripk1*^{EKO} *Zbp1*^{Za1a2/Za1a2} or 10–12-wk-old *Ripk1*^{EKO} *Zbp1*^{Za1a2/Za1a2} mice were activated with PMA and ionomycin and stained for intracellular expression of IFN γ and IL-17A. In B, representative flow cytometry plots are shown for each genotype. Panel C represents the number of IL-17A-positive immune cells per square centimeter of epidermis. Each dot represents an individual mouse, and the line represents the mean. **(D)** RT-qPCR analysis of *Il23a* in whole back skin of 4–5-wk-old mice of the indicated genotypes. Data in A–D are representative of two independent experiments. *, P < 0.05, **, P < 0.01, ***, P < 0.001 by Mann-Whitney U test.

et al., 2016), which may further contribute to skin inflammation. However, *Ripk1*^{EKO} *Casp1*/*Il-1*^{-/-} mice were indistinguishable from *Ripk1*^{EKO} littermates in terms of skin lesion development, thereby excluding a role for pyroptosis in skin pathology (Fig. 3 D). Together, these results show that sensing of nucleic acids by ZBP1 in keratinocytes of *Ripk1*^{EKO} mice causes MLKL-dependent necroptosis, which initiates skin inflammation.

ZBP1 activation by endogenous nucleic acids induces necroptosis in RIPK1-deficient keratinocytes

To establish if ZBP1 directly induced cell death of RIPK1-deficient keratinocytes, we treated primary RIPK1-deficient keratinocytes with type I (IFN β) or type II IFNs (IFN γ), which strongly induced ZBP1 protein levels (Fig. 4 A and Fig. S1 B), and monitored cell death by measuring uptake of a cell impermeable dye over a 48 h time course. At 12 h after treatment, RIPK1-deficient cells (*Ripk1*^{EKO} *Zbp1*^{+/+}) started to die, whereas RIPK1-

sufficient *Ripk1*^{FL/FL} *Zbp1*^{+/+} or *Ripk1*^{FL/FL} *Zbp1*^{Za1a2/Za1a2} keratinocytes were unaffected (Fig. 4 C). Immunoblotting revealed that IFN γ or IFN β treatment induced the phosphorylation of MLKL and RIPK3 only in cells that were lacking RIPK1 and expressing wild-type ZBP1 (Fig. 4 A). In contrast, keratinocytes derived from *Ripk1*^{EKO} *Zbp1*^{Za1a2/Za1a2} mice were fully resistant to IFN γ - or IFN β -induced cell death and did not show phosphorylation of MLKL and RIPK3 (Fig. 4, A and C). Lentiviral transduction of wild-type but not $Z\alpha$ -domain mutant ZBP1 (*ZBP1*^{Za1a2mut}) caused increased cell death of RIPK1-deficient keratinocytes starting at 24 h after transduction, compared with the empty vector control (Fig. S3, A and B). These data suggest that endogenous nucleic acids activate ZBP1 in the absence of RIPK1. TNF stimulation did not induce cell death or MLKL and RIPK3 phosphorylation in RIPK1-deficient keratinocytes, and treatment with poly(I:C), an agonist for TLR3 that signals via TRIF, only modestly sensitized cells to necroptosis and independently of nucleic acid sensing by ZBP1 (Fig. 4, B and C).

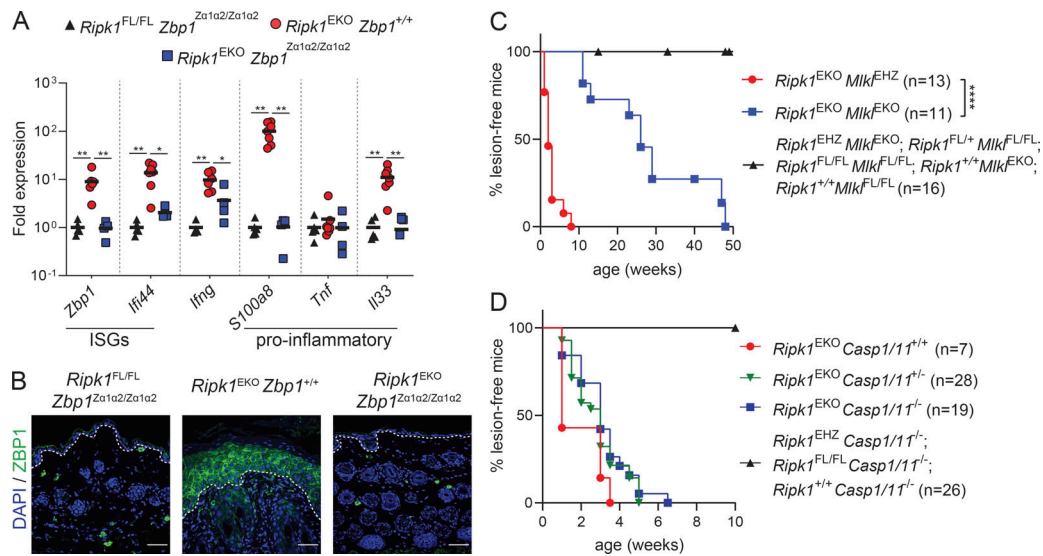


Figure 3. Induction of MLKL-dependent necroptosis by ZBP1 in keratinocytes drives skin inflammation in *Ripk1^{EKO}* mice. (A) RT-qPCR analysis of indicated ISGs, IFN γ , and pro-inflammatory genes in whole back skin of 4–5-wk-old mice of the indicated genotypes. The line represents the mean, and dots represent individual mice. *, P < 0.05 and **, P < 0.01 by Mann–Whitney U test. (B) Immunostaining with anti-ZBP1 on back skin sections from 5–7-wk-old *Ripk1^{FL/FL} Zbp1^{Za1a2/Za1a2}*, *Ripk1^{EKO} Zbp1^{+/+}*, or *Ripk1^{EKO} Zbp1^{Za1a2/Za1a2}* mice. Scale bars, 50 μ m. The dotted line indicates the border between the epidermis and dermis. At least four mice per genotype were analyzed. (C) Kaplan–Meier plot of macroscopically visible lesion appearance of epidermis-specific RIPK1 and MLKL double-deficient mice (*Ripk1^{EKO} Mkl^{EKO}*). *Ripk1^{EKO} Mkl^{EHZ}* mice, heterozygously expressing a functional *Mkl* allele in the epidermis in a *Ripk1^{EKO}* background, developed lesions at the same rate as *Ripk1^{EKO}* mice, as shown in Fig. 1 A. Littermate offspring of the indicated genotypes containing one or two functional *Ripk1* and/or *Mkl* alleles did not develop lesions and are shown as controls. ****, P < 0.0001 by log-rank test. (D) Kaplan–Meier plot of macroscopically visible lesion appearance of epidermis-specific RIPK1 and full-body caspase-1/11 double-deficient mice (*Ripk1^{EKO} Casp1/11^{-/-}*). Caspase-1/11-sufficient *Ripk1^{EKO} Casp1/11^{+/+}* or *Ripk1^{EKO} Casp1/11^{+/-}* mice developed lesions at the same rate as *Ripk1^{EKO} Casp1/11^{-/-}*. Littermate offspring of the indicated genotypes expressing one or two functional *Ripk1* alleles did not develop lesions and are shown as controls. Data shown in A and B are representative of at least two independent experiments.

These results suggest that RIPK1 deficiency greatly sensitizes keratinocytes to ZBP1-induced necroptosis, but not downstream of other RHIM-containing signaling complexes formed after TNF receptor 1 (TNFR1) stimulation and only modestly upon TLR3 engagement. The sensitization of RIPK1-deficient keratinocytes to TLR3/TRIF-mediated necroptosis may explain the mild amelioration of skin inflammation in *Ripk1^{EKO}* mice by epidermis-specific deletion of TRIF (Dannappel et al., 2014). As a control, treatment with a combination of TNF and the pan-caspase inhibitor carbobenzoxy-valyl-alanyl-aspartyl-[O-methyl]-fluoromethylketone (zVAD), which induces TNFR1-dependent necroptosis, only induced MLKL and RIPK3 phosphorylation and cell death in RIPK1-sufficient cells (Fig. 4 D and Fig. S3 C). Loss of RIPK1 sensitized keratinocytes to caspase-8-dependent apoptosis induced by treating cells with TNF and the protein synthesis inhibitor cycloheximide (CHX; Fig. 4 D and Fig. S3 C), which is in agreement with previous reports (Gentle et al., 2011; Kelliher et al., 1998). Spontaneous ZBP1 activation in RIPK1-deficient keratinocytes did not affect IFN γ -induced gene expression as ISG messenger RNA expression or CXCL10 protein production did not differ between the genotypes (Fig. S3, D and E).

In summary, we report that ZBP1 induces a cell-intrinsic ZBP1-RIPK3-MLKL pro-necroptotic signaling cascade in RIPK1-deficient keratinocytes resulting in inflammatory skin disease. Disease development in *Ripk1^{EKO}* mice depended on the nucleic acid sensing capacity of ZBP1, supporting the idea that endogenous

nucleic acids function as the upstream trigger for the execution of necroptosis. The molecular identity of the nucleic acid agonist of ZBP1 under these conditions remains unknown. Two lines of evidence favor the hypothesis that cellular nucleic acids, and not those of viral or bacterial origin, activate ZBP1. First, cultured primary RIPK1 keratinocytes, grown in sterile conditions, succumb to IFN-induced necroptosis, which crucially depended on the nucleic acid sensing capability of ZBP1. This is in agreement with earlier studies reporting on the toxicity of IFNs for RIPK1-deficient fibroblasts (Dillon et al., 2014; Kaiser et al., 2014), and which was recently shown to depend on ZBP1 (Ingram et al., 2019; Yang et al., 2020). Second, embryos expressing a mutant RIPK1 RHIM develop ZBP1-RIPK3-MLKL-driven inflammatory epidermal hyperplasia at embryonic day 18.5, before exposure to microbes at birth (Lin et al., 2016; Newton et al., 2016). Based on our observations in *Ripk1^{EKO}* mice, we anticipate that the embryonic lethality of RIPK1 RHIM mutant mice also requires nucleic acid sensing by ZBP1. It is not clear at which level RIPK1 operates to suppress ZBP1-mediated necroptosis. In the absence of an intact RHIM of RIPK1, RIPK3 spontaneously associates with ZBP1, suggesting that RIPK1 acts as a molecular scaffold to retain RIPK3 in an inactive state (Lin et al., 2016; Newton et al., 2016).

We and other groups identified ZBP1 as a sensor of viral RNA (Maelfait et al., 2017; Sridharan et al., 2017; Thapa et al., 2016). Our current data bring forward the hypothesis that the detection of endogenous nucleic acids by ZBP1 contributes to inflammatory

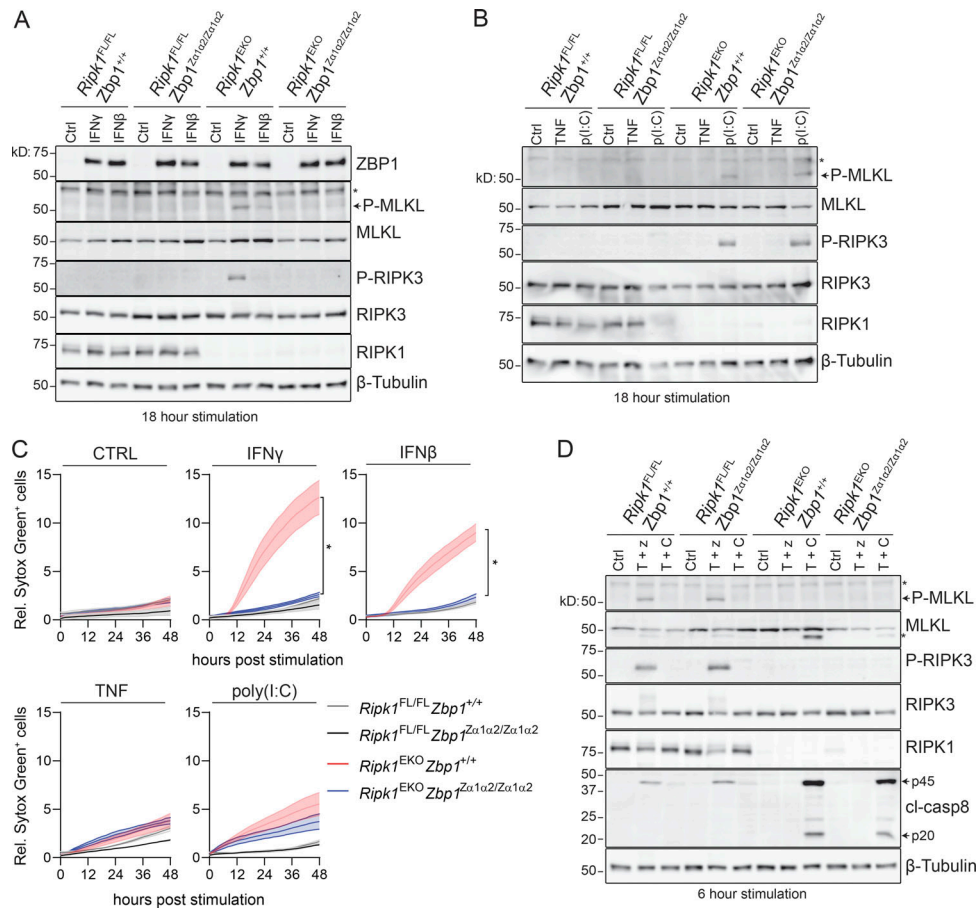


Figure 4. ZBP1 activation by endogenous nucleic acids induces necroptosis in RIPK1-deficient keratinocytes. (A, B, and D) Primary keratinocytes isolated from *Ripk1^{FL/FL} Zbp1^{+/+}*, *Ripk1^{FL/FL} Zbp1^{Za1a2/Za1a2}*, *Ripk1^{EKO} Zbp1^{+/+}*, or *Ripk1^{EKO} Zbp1^{Za1a2/Za1a2}* mice were stimulated for 18 h with 200 U/ml IFN γ , 200 U/ml IFN β , 30 ng/ml TNF, or 25 μ g/ml poly(I:C) [p(I:C)] or for 6 h with 30 ng/ml TNF with 20 μ M zVAD-fmk (T + z) or 30 ng/ml TNF with 5 μ g/ml CHX (T + C). Protein expression was analyzed by Western blotting. The asterisk (*) on the phospho(P)-MLKL blot indicates a nonspecific signal. The cleaved caspase-8 (cl-casp8) forms p45 and p20 are indicated with arrows. **(C)** Analysis of cell death upon stimulation with 200 U/ml IFN γ , 200 U/ml IFN β , 30 ng/ml TNF, or 25 μ g/ml poly(I:C) by measuring relative (Rel.) Sytox Green uptake every 2 h of primary keratinocytes isolated from mice of the indicated genotype. Solid lines represent the mean of cell death curves of two to four primary keratinocyte cultures isolated from different mice. Shaded areas indicate SEM. *, $P < 0.05$ by two-way ANOVA on data from *Ripk1^{EKO} Zbp1^{+/+}* ($n = 4$) and *Ripk1^{EKO} Zbp1^{Za1a2/Za1a2}* ($n = 4$) cultures. Data shown in A–D are representative of at least two independent experiments. Ctrl, control.

skin disease. Indeed, while this study was under review, two other groups reported that spontaneous activation of ZBP1 by endogenous nucleic acids caused skin and intestinal inflammation (Jiao et al., 2020; Wang et al., 2020). Whether RNA or DNA serve as agonists for ZBP1 in RIPK1-deficient keratinocytes remains to be determined. $Z\alpha$ -domains found in ZBP1 and the RNA editing enzyme ADAR1 specifically bind to nucleic acids in the Z-conformation, including Z-RNA and Z-DNA (Herbert, 2019). How dsRNA or dsDNA is stabilized in the thermodynamically unfavorable Z-conformation in living cells is unknown. At least in vitro, alternating CG rather than AT sequences more readily transition into the Z-conformation, suggesting that the sequence context is a contributing factor (Hall et al., 1984; Wang et al., 1979). Another possibility is that nucleic acid binding to ZBP1 promotes the stabilization of the Z-conformer. Indeed, the second $Z\alpha 2$ domain of ZBP1 binds B-form DNA and facilitates its transition into Z-DNA (Kim et al., 2011a, b). We cannot rule out that the mutation of the $Z\alpha$ -domains of ZBP1 affects other

functions of ZBP1 apart from nucleic acid binding. However, our data showing that ectopically expressed $Z\alpha$ -domain mutant ZBP1 still activates NF- κ B (Maelfait et al., 2017) and binds to RIPK3 (see Fig. S1 C) suggest that at least the RHIM-RHIM interactions between ZBP1 and RIPK3 remained intact.

Complete *Ripk1* knock-out mice die perinatally due to unconstrained activation of both apoptotic and necroptotic pathways (Dillon et al., 2014; Kaiser et al., 2014; Rickard et al., 2014b). At the epithelial barriers, there appears to be an interesting dichotomy in the survival functions of RIPK1. In intestinal epithelium, RIPK1 prevents cell death mediated by TNF and caspase-8-dependent apoptosis (Dannappel et al., 2014; Takahashi et al., 2014), whereas loss of RIPK1 in skin epithelial cells unleashes ZBP1-RIPK3-MLKL-mediated necroptosis (Dannappel et al., 2014). Why is one cell type more sensitive to apoptosis and another cell type more skewed toward necroptosis in the absence of RIPK1? A simple explanation may be the differential expression levels of components

of cell death pathways such as Fas-associated protein with death domain (FADD), caspase-8, RIPK3, and MLKL. However, this does not appear to be the case since keratinocyte-specific depletion of the linear ubiquitination chain assembly complex results in TNF/caspase-8-driven apoptosis driving dermatitis (Gerlach et al., 2011; Kumari et al., 2014; Rickard et al., 2014a; Taraborrelli et al., 2018). Vice versa, ablation of FADD or caspase-8 triggers necroptosis of intestinal epithelial cells, leading to chronic intestinal inflammation (Günther et al., 2011; Welz et al., 2011). A more complex scenario in which the mode of cell death is dictated by the availability of certain PRRs and their respective ligands together with regulatory mechanisms imprinted by the genetic background, the tissue environment, and/or inflammatory cues is more likely.

In most cell types, including keratinocytes, ZBP1 levels are undetectable under steady-state conditions, and its transcription is strongly induced by IFNs (Shaw et al., 2017). Here, we demonstrate that the skin of *Ripk1*^{EKO} mice displays an innate antiviral immune response, which is responsible for the high levels of ZBP1 expression. Cultured RIPK1-deficient keratinocytes, however, do not express enhanced ZBP1 levels, indicating that keratinocyte-intrinsic triggers do not provide the cues stimulating the antiviral immune response in the skin of *Ripk1*^{EKO} mice. Bacterial or viral colonization of the newborn epidermis during parturition may engage type-I IFN, inducing nucleic acid sensors in keratinocytes or in adjacent immune cells, inducing ZBP1 levels above a certain toxic threshold. In addition, damage-associated molecular patterns released by necroptotic cells can be detected by PRRs in neighboring cells, further supporting inflammation. Once the initial trigger is delivered, RIPK1-deficient keratinocytes undergoing ZBP1-dependent necroptosis may set in motion an auto-amplifying inflammatory signaling cascade establishing chronic inflammation. This is reminiscent of the chronic proliferative dermatitis phenotype of SHANK-associated RH domain interactor (SHARPIN)-deficient mice, where the initial trigger is TNF-induced keratinocyte cell death. Release of dsRNA from dying cells then activates TLR3, which in SHARPIN-deficient conditions causes cell death resulting in a self-promoting cycle of inflammation (Zinngrebe et al., 2016).

We demonstrate that keratinocyte necroptosis drives IL-17-mediated inflammation. A recent study showed that the transgenic expression of cFLIP_S, a splice variant of the cFLIP_L gene *Cflar*, caused the activation of ILC3s, which depended on necroptosis of intestinal epithelial cells (Shindo et al., 2019). At this stage, we do not know whether the IL-17 response is protective and aiding in tissue repair or whether it contributes to disease progression and chronic skin inflammation, as seen in patients with psoriasis (Brembilla et al., 2018; Ho and Kupper, 2019). Future studies in IL-23- or IL-17-deficient animals will provide clarity in this matter (Tait Wojno et al., 2019). Finally, our observations may assign important roles for endogenous nucleic acid sensing by ZBP1 in primary immunodeficiency and inflammatory disease observed in RIPK1-deficient patients (Cuchet-Lourenço et al., 2018; Li et al., 2019).

Materials and methods

Mice

Ripk1^{FL/FL} (Takahashi et al., 2014), Keratin-5-Cre (Ramirez et al., 2004), *Ripk3*^{-/-} (Newton et al., 2004), *Mkl1*^{FL/FL} (Murphy et al., 2013), *Zbp1*^{-/-} (Ishii et al., 2008), *Casp1/11*^{-/-} (Kuida et al., 1995), and *Zbp1*^{Za1a2/Za1a2} (Maelfait et al., 2017) mice were housed in individually ventilated cages at the VIB-UGent Center for Inflammation Research in a specific pathogen-free facility. *Casp1/11*^{-/-} mice were purchased from The Jackson Laboratory (B6N.129S2-Casp1^{tm1Flv/J}). *Ripk1*^{FL/FL}, *Mkl1*^{FL/FL}, and *Zbp1*^{Za1a2/Za1a2} mice were generated in C57Bl/6 embryonic stem (ES) cells, Keratin-5-Cre transgenes were generated in C57Bl/6jxDBA/2J ES cells, and *Ripk3*^{-/-}, *Casp1/11*^{-/-} (Kayagaki et al., 2015) and *Zbp1*^{-/-} (Koebler et al., 2020) mice were generated in 129-derived ES cells. All lines were maintained in a C57Bl/6 background. Mouse lines that were not generated in C57Bl/6 ES cells were backcrossed at least 10 times to a C57Bl/6 background. Littermates were used as controls for all experiments. All experiments were conducted following approval by the local Ethics Committee of Ghent University.

Reagents

Mouse TNF and mouse IFN γ were produced by the VIB Protein Service Facility. zVAD-fmk (Bachem; BACEN-1510.0005), CHX (Sigma-Aldrich; C7698), poly(I:C) (Invivogen; tlr-pic), mouse IFN β (PBL Biomedical Laboratories), and mouse CXCL10 ELISA (Thermo Fisher Scientific; BMS6018MST) were obtained from commercial sources.

Western blotting and immunoprecipitation

For Western blotting, cells were washed with PBS and lysed in protein lysis buffer (50 mM Tris HCl, pH 7.5, 1% Igepal CA-630, and 150 mM NaCl) supplemented with complete protease inhibitor cocktail (Roche; 11697498001) and PhosSTOP (Roche; 4906845001). Lysates were cleared by centrifugation at 16,000 *g* for 15 min, and 5 \times Laemmli loading buffer (250 mM Tris HCl, pH 6.8, 10% SDS, 0.5% Bromophenol blue, 50% glycerol, and 20% β -mercaptoethanol) was added to the supernatant. Finally, samples were incubated at 95°C for 5 min and analyzed using Tris-Glycine SDS-PAGE and semi-dry immunoblotting. For immunoprecipitation, HEK293T cells were transfected with Lipofectamine 2000 (Life Technologies) with N-terminally V5-tagged mouse ZBP1 and mouse RIPK3 cloned into pcDNA3 expression vectors. 24 h after transfection, cells were washed in PBS and lysed in protein lysis buffer. Lysates were cleared from debris by centrifugation at 16,000 *g* for 15 min, and 10% of the sample was used for input control. The remaining lysate was incubated overnight at 4°C on a rotating wheel using anti-V5 Affinity Gel beads (Sigma-Aldrich; A7345). Beads were washed three times with protein lysis buffer. Finally, the beads were resuspended in 1 \times Laemmli buffer and incubated at 95°C for 5 min. Primary antibodies used in this study are anti-ZBP1 (Adipogen; Zippy-1), anti-RIPK1 (CST; 3493), anti-RIPK3 (ProSci; 2283), anti-MLKL (Millipore; MABC604), anti-phospho-Thr231/Ser232-RIPK3 (CST; 57220), anti-phospho-S345-MLKL (Abcam; 196436), anti-V5-HRP (Invitrogen; R960-25), and anti- β -tubulin-HRP (Abcam; 21058).

Histology and immunohistochemistry

Back skin biopsy specimens were fixed in 4% paraformaldehyde in PBS overnight at 4°C, after which they were embedded in paraffin and sectioned at 5 μm thickness. Sections were deparaffinized before H&E staining using a Varistain Slide Stainer. For determining the epidermal thickness, H&E-stained skin sections with a length of ~1 cm were imaged with a ZEISS Axio Scan slide scanner. Then, the thickness of the epidermis was measured at 10 points per skin section with the ZEISS Blue software, and the values were expressed as the average of these 10 measurements. For immunofluorescence, sections were deparaffinized and rehydrated using a Varistain Slide Stainer. Antigen retrieval was performed by boiling sections at 95°C for 10 min in antigen retrieval solution (Vector; H-3301). Slides were then treated with 3% H₂O₂ in PBS for 10 min and 0.1 M NaBH₄ in PBS for 2 h at room temperature to reduce background. After washing in PBS, tissues were blocked in 1% BSA and 1% goat serum in PBS for 30 min at room temperature. Tissue sections were stained overnight at 4°C with following primary antibodies: anti-K6 (Covance; PRB-169P), anti-K5 (Covance; PRB-160P), anti-K1 (Covance; PRB-165P), and anti-ZBP1 (Adipogen; Zippy-1). Next, sections were incubated with donkey anti-mouse CF633 (Gentaur; 20124-1) or goat anti-rabbit DyLight488 (Thermo Fisher Scientific; 35552) and DAPI (Life Technologies; D1306) for 30 min at room temperature. Images were acquired on a Zeiss LSM880 Fast AiryScan confocal microscope using ZEN Software (Zeiss) and processed using Fiji (ImageJ).

Quantitative RT-PCR (RT-qPCR)

Snap-frozen back skin was homogenized on dry ice using a mortar and pestle. Total RNA was purified using RNeasy columns (Qiagen) with on-column DNase I digestion. cDNA synthesis was performed using the SensiFast cDNA synthesis kit (Bioline; BIO-65054). SensiFast SYBR No-Rox kit (Bioline; BIO-98005) or PrimeTime qPCR Master Mix (IDT; 1055771) was used for cDNA amplification using a Lightcycler 480 system (Roche). The following primers were used for SYBR-green based detection, and the median expression of *Rpl3a* and *Hprt* were used for normalization: *Ifng*, forward 5'-GCCAAGCGGCTGACTGA-3' and reverse 5'-TCAGTGAAGTAAAGGTACAAGCTACAATCT-3'; *S100a8*, forward 5'-GGAGTTCCTTGCGATGGTGAT-3' and reverse 5'-CAGCCCTAGGCCAGAAGCT-3'; *Tnf*, forward 5'-CCA CCACGCTCTTCTGTCTA-3' and reverse 5'-GCTACAGGCTTG TCACTCGAA-3'; *Il33*, forward 5'-GAGCATCCAAGGAACCTCAC-3' and reverse 5'-AGATGTCTGTGTCTTTGA-3'; *Isg15*, forward 5'-TGACGCAGACTGTAGACACG-3' and reverse 5'-TGGGGCTTT AGGCCATACTC-3'; *Ifit1*, forward 5'-CAGAAGCACACATTGAAG AA-3' and reverse 5'-TGTAAGTAGCCAGAGGAAGG-3'; *Cd20*, forward 5'-TGCTATCATCTTTACACGA-3' and reverse 5'-CAT CTTCTTGACTCTTAGGCTG-3'; *Il6*, forward 5'-TTCTCTGGGAAA TCGTGGAAA-3' and reverse 5'-TCAGAATTGCCATTGCACAAC-3'; *Il1a*, forward 5'-CCTGCAGTCCATAACCCATGA-3' and reverse 5'-ACTTCTGCCTGACGAGCTTCA-3'; *Il1b*, forward 5'-CCAAAA GATGAAGGGCTGCTT-3' and reverse 5'-TCATCAGGACAGCC AGGTC-3'; *Rpl3a*, forward 5'-CCTGCTGCTCTCAAGTTGTT-3' and reverse 5'-TGTTGCTACTGCCTGGTACTT-3' and *Hprt*,

forward 5'-CAAGCTTGCTGGTAAAAGGA-3' and reverse 5'-TGCGCTCATCTTAGGCTTTGTA-3'. The following oligos were purchased from IDT for probe-based detection, and the median expression of *Tbp* and *Actb* were used for normalization: *Zbp1*, Mm.PT.58.21951435; *Ifi44*, Mm.PT.58.12162024, *Tbp*, Mm.PT.39a.22214839; and *Actb*, Mm.PT.39a.22214843.g.

Primary keratinocytes cultures

Primary keratinocytes were isolated from back skin of 4–5-wk-old mice. Back skin was shaved with electrical clippers and sterilized with 10% betadine and 70% ethanol. Subcutaneous fat and muscles were removed by mechanical scrapping. Subsequently, the skin was carefully placed on 0.25% trypsin (GIBCO BRL; 25050014) with dermal side downward for 2 h at 37°C. Epidermis was separated from the dermis with a forceps, cut into fine pieces, and incubated in fresh 0.25% trypsin for 5 min at 37°C with rotation. After neutralization with supplemented FAD medium (see below), the epidermal cell suspension was filtered through a 70 μm cell strainer. The keratinocytes were seeded on J2 3T3 feeder cells that were mitotically inactivated by treatment with 4 μg/ml Mitomycin C (Sigma-Aldrich; #M-0503) for 2 h, in 1 μg/ml collagen I-coated falcons (Sigma-Aldrich; 5006). Keratinocytes were cultured at 32°C in a humidified atmosphere of 5% CO₂, and medium was replaced every 2 d. After 12–14 d, the remaining J2 3T3 feeder cells were removed from the culture by short incubation with 0.25% trypsin, and the keratinocytes were harvested subsequently. Keratinocytes were seeded at a density of 25,000 cells per cm² into collagen I-coated culture plates for cell death measurements (48-well) and Western blot analysis (12-well). Primary mouse keratinocytes were cultured in custom-made (Biochrom, Merck) DMEM/Ham's F12 (FAD) medium with low Ca²⁺ (50 μM) supplemented with 10% FCS (Gibco) treated with chelex 100 resin (Bio-Rad; 142-2832), 0.18 mM adenine (Sigma-Aldrich; A2786), 0.5 μg/ml hydrocortisone (Sigma-Aldrich; H4001), 5 μg/ml insulin (Sigma-Aldrich; I3536), 10⁻¹⁰ M cholera toxin (Sigma-Aldrich; C8052), 10 ng/ml epidermal growth factor (Thermo Fisher Scientific; 53003018), 2 mM glutamine (Lonza; BE17-605F), 1 mM pyruvate (Sigma-Aldrich; S8636), 100 U/ml penicillin and 100 μg/ml streptomycin (Sigma-Aldrich; P4333), and 16 μg/ml gentamycin (GIBCO BRL; 15710064).

Cell death assays

25,000 primary keratinocytes were seeded per well in 1 μg/ml collagen I-coated 48-well plates in FAD medium. 24 h later, the cell-impermeable dye SYTOX Green (1 μM, Thermo Fisher Scientific; S7020) was added to the culture medium together with the indicated stimuli. SYTOX Green uptake was imaged every 2 or 3 h with an IncuCyte Live-Cell Analysis system (Essen BioScience) at 37°C. The relative percentage of SYTOX Green cells was determined by dividing the number of SYTOX Green-positive cells per image by the percentage of confluency (using phase contrast images) at every time point.

Keratinocyte transduction

HEK293T were cultured in high-glucose (4,500 mg/liter) DMEM (GIBCO BRL; 41965-039) supplemented with 10% FCS and 2 mM

glutamine (Lonza; BE17-605F). For lentivirus production, HEK293T cells were transfected with N-terminally 3XFLAG and V5-tagged wild-type mouse ZBP1 or *Zα1a2* mutant mouse ZBP1 transducing vectors in the pLenti6 backbone (Life Technologies; Maelfait et al., 2017) together with the pCMV delta R8.91 gag-pol-expressing packaging plasmids and pMD2.G VSV-G-expressing envelope plasmid. 24 h after transfection, cells were washed and FAD medium was added. 48 h after transfection, the viral supernatant was harvested and used to transduce 25,000 mouse primary keratinocytes seeded in 48-well plates in the presence of 8 μg/ml polybrene (Sigma-Aldrich). The next day, viral particle-containing medium was removed, and cell death was measured for 48 h as described above.

Skin processing for flow cytometry analysis

A piece of shaved mouse skin (±12 cm²) was isolated from 4–5-wk-old mice. Subcutaneous fat and muscles were removed by mechanical scrapping with a scalpel. Subsequently, the skin was carefully placed on 0.4 mg/ml Dispase II (Roche; 4492078001) with the dermal side facing downward for 2 h at 37°C. Epidermis was separated from the dermis with a forceps, cut into fine pieces, and incubated in 2 ml enzymatic solution containing 1.5 mg/ml collagenase type IV (Worthington; LS004188) and 0.5 mg/ml Dnase I (Roche; 10104159001) for 20 min at 37°C with shaking. After neutralization with 2% FCS RPMI medium, the cell suspension was filtered through a 70 μm cell strainer to obtain a single cell suspension. For detection of intercellular cytokines, *in vitro* activation was performed. Single cell suspension from epidermis was seeded into 96-well U-bottom plate in RPMI 1640 medium supplemented with 10% FCS, 2 mM glutamine (Lonza; BE17-605F), 1 mM sodium pyruvate (Sigma-Aldrich; S8636), 100 U/ml penicillin and 100 μg/ml streptomycin (Sigma-Aldrich; P4333), and 50 mM β-mercaptoethanol (GIBCO BRL; 31350-010). Subsequently, the cell suspension was stimulated with eBioscience Cell Stimulation Cocktail plus protein transport inhibitor (eBioscience; 00-4975-03) for 4 h at 37°C in a humidified 5% CO₂ incubator.

Flow cytometry

Single cell suspensions were first stained with anti-mouse CD16/CD32 (Fc-block; BD Biosciences; 553142), and dead cells were excluded with the Fixable Viability Dye eFluor506 (eBioscience; 65-0866-14) for 30 min at 4°C in PBS. Next, cell surface markers were stained for 30 min at 4°C in FACS buffer (PBS, 5% FCS, 1 mM EDTA, and 0.05 sodium azide). For intracellular cytokine analysis, cells were fixed for 20 min at 4°C using BD Cytofix/Cytoperm (BD Biosciences; 554714) and washed twice with BD Perm/Wash buffer (BD Biosciences; 554714). Intracellular IFNγ and IL-17A were stained in BD Perm/Wash Buffer for 30 min at 4°C. Cells were acquired with on an LSR Fortessa or a FAC-Symphony (BD Biosciences), and data were analyzed with FlowJo software (Tree Star). The total number of cells was counted using a FACSVerse (BD Biosciences). The following fluorochrome-conjugated antibodies were used: CD3e#BUV395 (1/100; 563565), CD161#BV605 (1/300; 563220), CD4#FITC (1/400; 557307), TCRγδ#PECF594 (1/500; 563532), CD11b#PerCP-Cy5.5 (1/1,000; 550993), and CD44#PE (1/400; 553134) were

from BD Biosciences. CD8α#eFluor450 (1/400; 48-0081-82), CD45#AF700 (1/200; 56-0451), MHC Class II (I-A/I-E)#FITC (1/1,000; 11-5321), CD11c#PE-Cy7 (1/500; 25-0114-82), and IL17A#APC (1/200; 17-7177-81) were from eBioscience. CD19#BV785 (1/400; 115543), CD11c#BV785 (1/200; 117336), Ter-119#BV785 (1/400; 116245), Ly-6G#BV785 (1/400; 127645), TCRβ#APC-Cy7 (1/200; 109220), CD64(FcγRI)#BV711 (1/100; 139311), and IFNγ#PE/Cy7 (1/300; 505825) were from Biolegend.

Statistical analyses

Statistical analyses were performed using Prism 8.2.1 (GraphPad Software). Statistical methods are described in the figure legends.

Online supplemental material

Fig. S1 provides additional information for Fig. 1 and shows pictures of skin lesions of *Ripki*^{EKO} *Zbp1*^{+/+} and *Ripki*^{EKO} *Zbp1*^{Zα1a2/Zα1a2} mice, demonstrates equal protein expression of ZBP1 and Zα-domain mutant ZBP1 in RIPK1-deficient keratinocytes, and shows lesion formation of *Ripki*^{EKO} mice crossed to *Zbp1*^{-/-} and *Ripk3*^{-/-} animals. Fig. S2 relates to Fig. 2 and Fig. 3 and shows the gating strategy for Fig. 2 A and additional RT-qPCR analyses of ISGs and pro-inflammatory genes in the skin of *Ripki*^{EKO} *Zbp1*^{+/+} and *Ripki*^{EKO} *Zbp1*^{Zα1a2/Zα1a2} mice. Fig. S3 relates to Fig. 4 and describes cell death induction of RIPK1-deficient primary keratinocytes after transduction with ZBP1 or after treatment with TNF + zVAD or TNF + CHX. Fig. S3 also shows that ISG expression in keratinocytes upon IFNγ treatment is not affected by RIPK1 deficiency or Zα-domain mutation of ZBP1.

Acknowledgments

We are grateful to Kim Newton and Vishva Dixit (Genentech, San Francisco, CA) for providing *Ripk3*^{-/-} mice, to James Murphy and Warren Alexander (the Walter and Eliza Hall Institute of Medical Research, Parkville, Australia) for providing *Mkl1*^{FL/FL} mice, and to Ken Ishii and Shizuo Akira (Osaka University, Osaka, Japan) for providing *Zbp1*^{-/-} animals. We thank the members of the VIB Flow Core, Protein Service Facility, and the Microscopy Core, and Kelly Lemeire for technical assistance. We thank members of the Rehwinkel and Vandenabeele laboratory, Sophie Janssens, and Mathieu Bertrand for helpful discussions.

This research would not have been possible without support from the following funding agencies. J. Maelfait was supported by a Research Foundation Flanders Odysseus II Grant (GOH8618N) and by Ghent University. The W. Declercq laboratory was supported by "Vlaams Instituut voor Biotechnologie," a grant from Ghent University (GOA-01G01914), and a grant from "Stichting tegen Kanker" (FAF-F/2016/868). Research in the P. Vandenabeele unit is supported by a Research Foundation Flanders EOS grant (EOS 30826052 MODEL-IDI), Research Foundation Flanders grants (FWO G.OC31.14N, G.OC37.14N, FWO GOE04.16N, G.OC76.18N, G.OB71.18N, GOB9620N), a grant from Ghent University (BOF16/MET_V/007 Methusalem grant), a grant from the Foundation Against Cancer (FAF-F/2016/865), and by "Vlaams Instituut voor Biotechnologie." J. Rehwinkel is funded

by the UK Medical Research Council (MRC core funding of the MRC Human Immunology Unit).

Author contributions: M. Devos, G. Tanghe, P. Vandenabeele, W. Declercq, and J. Maelfait designed the study. M. Devos, G. Tanghe, B. Gilbert, E. Dierick, M. Verheirstraeten, J. Nemegeer, R. de Reuver, S. Lefebvre, J. De Munck, and J. Maelfait carried out the experiments. J. Rehwinkel provided critical reagents and scientific advice. M. Devos, G. Tanghe, B. Gilbert, W. Declercq, and J. Maelfait analyzed the results. M. Devos, G. Tanghe, W. Declercq, and J. Maelfait wrote the manuscript.

Disclosures: The authors declare no competing interests exist.

Submitted: 8 October 2019

Revised: 15 March 2020

Accepted: 8 April 2020

References

- Brembilla, N.C., L. Senra, and W.H. Boehncke. 2018. The IL-17 Family of Cytokines in Psoriasis: IL-17A and Beyond. *Front. Immunol.* 9:1682. <https://doi.org/10.3389/fimmu.2018.01682>
- Crow, Y.J., B.E. Hayward, R. Parmar, P. Robins, A. Leitch, M. Ali, D.N. Black, H. van Bokhoven, H.G. Brunner, B.C. Hamel, et al. 2006. Mutations in the gene encoding the 3'-5' DNA exonuclease TREX1 cause Aicardi-Goutières syndrome at the AGS1 locus. *Nat. Genet.* 38:917-920. <https://doi.org/10.1038/ng1845>
- Crowl, J.T., E.E. Gray, K. Pestal, H.E. Volkman, and D.B. Stetson. 2017. Intracellular Nucleic Acid Detection in Autoimmunity. *Annu. Rev. Immunol.* 35: 313-336. <https://doi.org/10.1146/annurev-immunol-051116-052331>
- Cuchet-Lourenço, D., D. Eletto, C. Wu, V. Plagnol, O. Papapietro, J. Curtis, L. Ceron-Gutierrez, C.M. Bacon, S. Hackett, B. Alsalem, et al. 2018. Biallelic RIPK1 mutations in humans cause severe immunodeficiency, arthritis, and intestinal inflammation. *Science.* 361:810-813. <https://doi.org/10.1126/science.aar2641>
- Dannappel, M., K. Vlantis, S. Kumari, A. Polykratis, C. Kim, L. Wachsmuth, C. Eftychi, J. Lin, T. Corona, N. Hermance, et al. 2014. RIPK1 maintains epithelial homeostasis by inhibiting apoptosis and necroptosis. *Nature.* 513:90-94. <https://doi.org/10.1038/nature13608>
- Dillon, C.P., R. Weinlich, D.A. Rodriguez, J.G. Cripps, G. Quarato, P. Gurung, K.C. Verbist, T.L. Brewer, F. Llambi, Y.N. Gong, et al. 2014. RIPK1 blocks early postnatal lethality mediated by caspase-8 and RIPK3. *Cell.* 157: 1189-1202. <https://doi.org/10.1016/j.cell.2014.04.018>
- Galluzzi, L., A. Buqué, O. Kepp, L. Zitvogel, and G. Kroemer. 2017. Immunogenic cell death in cancer and infectious disease. *Nat. Rev. Immunol.* 17:97-111. <https://doi.org/10.1038/nri.2016.107>
- Gentle, I.E., W.W. Wong, J.M. Evans, A. Bankovacki, W.D. Cook, N.R. Khan, U. Nachbur, J. Rickard, H. Anderton, M. Moulin, et al. 2011. In TNF-stimulated cells, RIPK1 promotes cell survival by stabilizing TRAF2 and cIAP1, which limits induction of non-canonical NF- κ B and activation of caspase-8. *J. Biol. Chem.* 286:13282-13291. <https://doi.org/10.1074/jbc.M110.216226>
- Gerlach, B., S.M. Cordier, A.C. Schmukle, C.H. Emmerich, E. Rieser, T.L. Haas, A.I. Webb, J.A. Rickard, H. Anderton, W.W. Wong, et al. 2011. Linear ubiquitination prevents inflammation and regulates immune signaling. *Nature.* 471:591-596. <https://doi.org/10.1038/nature09816>
- Günther, C., E. Martini, N. Wittkopf, K. Amann, B. Weigmann, H. Neumann, M.J. Waldner, S.M. Hedrick, S. Tenzer, M.F. Neurath, and C. Becker. 2011. Caspase-8 regulates TNF- α -induced epithelial necroptosis and terminal ileitis. *Nature.* 477:335-339. <https://doi.org/10.1038/nature10400>
- Guo, H., R.P. Gilley, A. Fisher, R. Lane, V.J. Landsteiner, K.B. Ragan, C.M. Dovey, J.E. Carette, J.W. Upton, E.S. Mocarski, and W.J. Kaiser. 2018. Species-independent contribution of ZBP1/DAI/DLM-1-triggered necroptosis in host defense against HSV1. *Cell Death Dis.* 9:816. <https://doi.org/10.1038/s41419-018-0868-3>
- Hall, K., P. Cruz, I. Tinoco Jr., T.M. Jovin, and J.H. van de Sande. 1984. 'Z-RNA'-a left-handed RNA double helix. *Nature.* 311:584-586. <https://doi.org/10.1038/311584a0>

- Herbert, A. 2019. Z-DNA and Z-RNA in human disease. *Commun. Biol.* 2:7. <https://doi.org/10.1038/s42003-018-0237-x>
- Ho, A.W., and T.S. Kupper. 2019. T cells and the skin: from protective immunity to inflammatory skin disorders. *Nat. Rev. Immunol.* 19:490-502. <https://doi.org/10.1038/s41577-019-0162-3>
- Ingram, J.P., R.J. Thapa, A. Fisher, B. Tummers, T. Zhang, C. Yin, D.A. Rodriguez, H. Guo, R. Lane, R. Williams, et al. 2019. ZBP1/DAI Drives RIPK3-Mediated Cell Death Induced by IFNs in the Absence of RIPK1. *J. Immunol.* 203:1348-1355. <https://doi.org/10.4049/jimmunol.1900216>
- Ishii, K.J., T. Kawagoe, S. Koyama, K. Matsui, H. Kumar, T. Kawai, S. Uematsu, O. Takeuchi, F. Takeshita, C. Coban, and S. Akira. 2008. TANK-binding kinase-1 delineates innate and adaptive immune responses to DNA vaccines. *Nature.* 451:725-729. <https://doi.org/10.1038/nature06537>
- Jeremiah, N., B. Neven, M. Gentili, I. Callebaut, S. Maschalidi, M.C. Stolzenberg, N. Goudin, M.L. Frémond, P. Nitschke, T.J. Molina, et al. 2014. Inherited STING-activating mutation underlies a familial inflammatory syndrome with lupus-like manifestations. *J. Clin. Invest.* 124:5516-5520. <https://doi.org/10.1172/JCI79100>
- Jiao, H., L. Wachsmuth, S. Kumari, R. Schwarzer, J. Lin, R.O. Eren, A. Fisher, R. Lane, G.R. Young, G. Kassiotis, et al. 2020. Z-nucleic-acid sensing triggers ZBP1-dependent necroptosis and inflammation. *Nature.* <https://doi.org/10.1038/s41586-020-2129-8>
- Kaiser, W.J., L.P. Daley-Bauer, R.J. Thapa, P. Mandal, S.B. Berger, C. Huang, A. Sundararajan, H. Guo, L. Roback, S.H. Speck, et al. 2014. RIP1 suppresses innate immune necrotic as well as apoptotic cell death during mammalian parturition. *Proc. Natl. Acad. Sci. USA.* 111:7753-7758. <https://doi.org/10.1073/pnas.1401857111>
- Kayagaki, N., I.B. Stowe, B.L. Lee, K. O'Rourke, K. Anderson, S. Warming, T. Cuellar, B. Haley, M. Roose-Girma, Q.T. Phung, et al. 2015. Caspase-11 cleaves gasdermin D for non-canonical inflammasome signalling. *Nature.* 526:666-671. <https://doi.org/10.1038/nature15541>
- Kelliher, M.A., S. Grimm, Y. Ishida, F. Kuo, B.Z. Stanger, and P. Leder. 1998. The death domain kinase RIP mediates the TNF-induced NF- κ B signal. *Immunity.* 8:297-303. [https://doi.org/10.1016/S1074-7613\(00\)80535-X](https://doi.org/10.1016/S1074-7613(00)80535-X)
- Kesavardhana, S., T. Kuriakose, C.S. Guy, P. Samir, R.K.S. Malireddi, A. Mishra, and T.D. Kanneganti. 2017. ZBP1/DAI ubiquitination and sensing of influenza vRNPs activate programmed cell death. *J. Exp. Med.* 214:2217-2229. <https://doi.org/10.1084/jem.20170550>
- Kim, H.E., H.C. Ahn, Y.M. Lee, E.H. Lee, Y.J. Seo, Y.G. Kim, K.K. Kim, B.S. Choi, and J.H. Lee. 2011a. The Z β domain of human DAI binds to Z-DNA via a novel B-Z transition pathway. *FEBS Lett.* 585:772-778. <https://doi.org/10.1016/j.febslet.2011.01.043>
- Kim, K., B.I. Khayrutdinov, C.K. Lee, H.K. Cheong, S.W. Kang, H. Park, S. Lee, Y.G. Kim, J. Jee, A. Rich, et al. 2011b. Solution structure of the Zbeta domain of human DNA-dependent activator of IFN-regulatory factors and its binding modes to B- and Z-DNAs. *Proc. Natl. Acad. Sci. USA.* 108: 6921-6926. <https://doi.org/10.1073/pnas.1014898107>
- Koehler, H.S., Y. Feng, P. Mandal, and E.S. Mocarski. 2020. Recognizing limits of Z-nucleic acid binding protein (ZBP1/DAI/DLM1) function. *FEBS J.* febs.15242. <https://doi.org/10.1111/febs.15242>
- Kuida, K., J.A. Lippke, G. Ku, M.W. Harding, D.J. Livingston, M.S. Su, and R.A. Flavell. 1995. Altered cytokine export and apoptosis in mice deficient in interleukin-1 beta converting enzyme. *Science.* 267:2000-2003. <https://doi.org/10.1126/science.7535475>
- Kumari, S., Y. Redouane, J. Lopez-Mosqueda, R. Shiraishi, M. Romanowska, S. Lutzmayer, J. Kuiper, C. Martinez, I. Dikic, M. Pasparakis, and F. Ikeda. 2014. Sharpin prevents skin inflammation by inhibiting TNFR1-induced keratinocyte apoptosis. *eLife.* 3:e03422. <https://doi.org/10.7554/eLife.03422>
- Kuriakose, T., and T.D. Kanneganti. 2018. ZBP1: Innate Sensor Regulating Cell Death and Inflammation. *Trends Immunol.* 39:123-134. <https://doi.org/10.1016/j.it.2017.11.002>
- Kuriakose, T., S.M. Man, R.K. Malireddi, R. Karki, S. Kesavardhana, D.E. Place, G. Neale, P. Vogel, and T.D. Kanneganti. 2016. ZBP1/DAI is an innate sensor of influenza virus triggering the NLRP3 inflammasome and programmed cell death pathways. *Sci. Immunol.* 1:aag2045. <https://doi.org/10.1126/sciimmunol.aag2045>
- Lee-Kirsch, M.A. 2017. The Type I Interferonopathies. *Annu. Rev. Med.* 68: 297-315. <https://doi.org/10.1146/annurev-med-050715-104506>
- Li, Y., M. Führer, E. Bahrami, P. Socha, M. Klaudel-Dreszler, A. Bouzidi, Y. Liu, A.S. Lehle, T. Magg, S. Hollizeck, et al. 2019. Human RIPK1 deficiency causes combined immunodeficiency and inflammatory bowel diseases. *Proc. Natl. Acad. Sci. USA.* 116:970-975. <https://doi.org/10.1073/pnas.1811582116>

- Lin, J., S. Kumari, C. Kim, T.M. Van, L. Wachsmuth, A. Polykratis, and M. Pasparakis. 2016. RIPK1 counteracts ZBP1-mediated necroptosis to inhibit inflammation. *Nature*. 540:124–128. <https://doi.org/10.1038/nature20558>
- Liu, Y., A.A. Jesus, B. Marrero, D. Yang, S.E. Ramsey, G.A.M. Sanchez, K. Tenbrock, H. Wittkowski, O.Y. Jones, H.S. Kuehn, et al. 2014. Activated STING in a vascular and pulmonary syndrome. *N. Engl. J. Med.* 371: 507–518. <https://doi.org/10.1056/NEJMoal312625>
- Maelfait, J., L. Liverpool, A. Bridgeman, K.B. Ragan, J.W. Upton, and J. Rehwinkel. 2017. Sensing of viral and endogenous RNA by ZBP1/DAI induces necroptosis. *EMBO J.* 36:2529–2543. <https://doi.org/10.15252/embj.201796476>
- Murphy, J.M., P.E. Czabotar, J.M. Hildebrand, I.S. Lucet, J.G. Zhang, S. Alvarez-Diaz, R. Lewis, N. Lalaoui, D. Metcalf, A.I. Webb, et al. 2013. The pseudokinase MLKL mediates necroptosis via a molecular switch mechanism. *Immunity*. 39:443–453. <https://doi.org/10.1016/j.immuni.2013.06.018>
- Newton, K., and G. Manning. 2016. Necroptosis and Inflammation. *Annu. Rev. Biochem.* 85:743–763. <https://doi.org/10.1146/annurev-biochem-060815-014830>
- Newton, K., X. Sun, and V.M. Dixit. 2004. Kinase RIP3 is dispensable for normal NF-kappa Bs, signaling by the B-cell and T-cell receptors, tumor necrosis factor receptor 1, and Toll-like receptors 2 and 4. *Mol. Cell. Biol.* 24:1464–1469. <https://doi.org/10.1128/MCB.24.4.1464-1469.2004>
- Newton, K., K.E. Wickliffe, A. Maltzman, D.L. Dugger, A. Strasser, V.C. Pham, J.R. Lill, M. Roose-Girma, S. Warming, M. Solon, et al. 2016. RIPK1 inhibits ZBP1-driven necroptosis during development. *Nature*. 540: 129–133. <https://doi.org/10.1038/nature20559>
- Nielsen, M.M., D.A. Witherden, and W.L. Havran. 2017. $\gamma\delta$ T cells in homeostasis and host defence of epithelial barrier tissues. *Nat. Rev. Immunol.* 17:733–745. <https://doi.org/10.1038/nri.2017.101>
- Pasparakis, M., and P. Vandenabeele. 2015. Necroptosis and its role in inflammation. *Nature*. 517:311–320. <https://doi.org/10.1038/nature14191>
- Ramirez, A., A. Page, A. Gandarillas, J. Zanet, S. Pibre, M. Vidal, L. Tusell, A. Genesca, D.A. Whitaker, D.W. Melton, and J.L. Jorcano. 2004. A keratin K5Cre transgenic line appropriate for tissue-specific or generalized Cre-mediated recombination. *Genesis*. 39:52–57. <https://doi.org/10.1002/gene.20025>
- Rice, G.I., J. Bond, A. Asipu, R.L. Brunette, I.W. Manfield, I.M. Carr, J.C. Fuller, R.M. Jackson, T. Lamb, T.A. Briggs, et al. 2009. Mutations involved in Aicardi-Goutières syndrome implicate SAMHD1 as regulator of the innate immune response. *Nat. Genet.* 41:829–832. <https://doi.org/10.1038/ng.373>
- Rice, G.I., P.R. Kashner, G.M. Forte, N.M. Mannion, S.M. Greenwood, M. Szykiewicz, J.E. Dickerson, S.S. Bhaskar, M. Zampini, T.A. Briggs, et al. 2012. Mutations in ADAR1 cause Aicardi-Goutières syndrome associated with a type I interferon signature. *Nat. Genet.* 44:1243–1248. <https://doi.org/10.1038/ng.2414>
- Rice, G.I., Y. Del Toro Duany, E.M. Jenkinson, G.M. Forte, B.H. Anderson, G. Ariaudo, B. Bader-Meunier, E.M. Baildam, R. Battini, M.W. Beresford, et al. 2014. Gain-of-function mutations in IFIH1 cause a spectrum of human disease phenotypes associated with upregulated type I interferon signaling. *Nat. Genet.* 46:503–509. <https://doi.org/10.1038/ng.2933>
- Rickard, J.A., H. Anderton, N. Etemadi, U. Nachbur, M. Darding, N. Peltzer, N. Lalaoui, K.E. Lawlor, H. Vanyai, C. Hall, et al. 2014a. TNFR1-dependent cell death drives inflammation in Sharpin-deficient mice. *eLife*. 3: e03464. <https://doi.org/10.7554/eLife.03464>
- Rickard, J.A., J.A. O'Donnell, J.M. Evans, N. Lalaoui, A.R. Poh, T. Rogers, J.E. Vince, K.E. Lawlor, R.L. Ninnis, H. Anderton, et al. 2014b. RIPK1 regulates RIPK3-MLKL-driven systemic inflammation and emergency hematopoiesis. *Cell*. 157:1175–1188. <https://doi.org/10.1016/j.cell.2014.04.019>
- Rodero, M.P., and Y.J. Crow. 2016. Type I interferon-mediated monogenic autoinflammation: The type I interferonopathies, a conceptual overview. *J. Exp. Med.* 213:2527–2538. <https://doi.org/10.1084/jem.20161596>
- Shaw, A.E., J. Hughes, Q. Gu, A. Behdenna, J.B. Singer, T. Dennis, R.J. Orton, M. Varela, R.J. Gifford, S.J. Wilson, and M. Palmarini. 2017. Fundamental properties of the mammalian innate immune system revealed by multispecies comparison of type I interferon responses. *PLoS Biol.* 15: e2004086. <https://doi.org/10.1371/journal.pbio.2004086>
- Shindo, R., M. Ohmuraya, S. Komazawa-Sakon, S. Miyake, Y. Deguchi, S. Yamazaki, T. Nishina, T. Yoshimoto, S. Kakuta, M. Koike, et al. 2019. Necroptosis of Intestinal Epithelial Cells Induces Type 3 Innate Lymphoid Cell-Dependent Lethal Ileitis. *iScience*. 15:536–551. <https://doi.org/10.1016/j.isci.2019.05.011>
- Sridharan, H., K.B. Ragan, H. Guo, R.P. Gilley, V.J. Landsteiner, W.J. Kaiser, and J.W. Upton. 2017. Murine cytomegalovirus IE3-dependent transcription is required for DAI/ZBP1-mediated necroptosis. *EMBO Rep.* 18: 1429–1441. <https://doi.org/10.15252/embr.201743947>
- Tait Wojno, E.D., C.A. Hunter, and J.S. Stumhofer. 2019. The Immunobiology of the Interleukin-12 Family: Room for Discovery. *Immunity*. 50: 851–870. <https://doi.org/10.1016/j.immuni.2019.03.011>
- Takahashi, N., L. Vereecke, M.J. Bertrand, L. Duprez, S.B. Berger, T. Divert, A. Gonçalves, M. Sze, B. Gilbert, S. Kourula, et al. 2014. RIPK1 ensures intestinal homeostasis by protecting the epithelium against apoptosis. *Nature*. 513:95–99. <https://doi.org/10.1038/nature13706>
- Taraborrelli, L., N. Peltzer, A. Montinaro, S. Kupka, E. Rieser, T. Hartwig, A. Sarr, M. Darding, P. Draber, T.L. Haas, et al. 2018. LUBAC prevents lethal dermatitis by inhibiting cell death induced by TNF, TRAIL and CD95L. *Nat. Commun.* 9:3910. <https://doi.org/10.1038/s41467-018-06155-8>
- Thapa, R.J., J.P. Ingram, K.B. Ragan, S. Nogusa, D.F. Boyd, A.A. Benitez, H. Sridharan, R. Kosoff, M. Shubina, V.J. Landsteiner, et al. 2016. DAI Senses Influenza A Virus Genomic RNA and Activates RIPK3-Dependent Cell Death. *Cell Host Microbe*. 20:674–681. <https://doi.org/10.1016/j.chom.2016.09.014>
- Upton, J.W., W.J. Kaiser, and E.S. Mocarski. 2012. DAI/ZBP1/DLM-1 complexes with RIP3 to mediate virus-induced programmed necrosis that is targeted by murine cytomegalovirus vIRA. *Cell Host Microbe*. 11:290–297. <https://doi.org/10.1016/j.chom.2012.01.016>
- Wallach, D., T.B. Kang, C.P. Dillon, and D.R. Green. 2016. Programmed necrosis in inflammation: Toward identification of the effector molecules. *Science*. 352:aaf2154. <https://doi.org/10.1126/science.aaf2154>
- Wang, A.H., G.J. Quigley, F.J. Kolpak, J.L. Crawford, J.H. van Boom, G. van der Marel, and A. Rich. 1979. Molecular structure of a left-handed double helical DNA fragment at atomic resolution. *Nature*. 282:680–686. <https://doi.org/10.1038/282680a0>
- Wang, R., H. Li, J. Wu, Z.-Y. Cai, B. Li, H. Ni, X. Qiu, H. Chen, W. Liu, Z.-H. Yang, et al. 2020. Gut stem cell necroptosis by genome instability triggers bowel inflammation. *Nature*. 580:386–390. <https://doi.org/10.1038/s41586-020-2127-x>
- Weinlich, R., A. Oberst, H.M. Beere, and D.R. Green. 2017. Necroptosis in development, inflammation and disease. *Nat. Rev. Mol. Cell Biol.* 18: 127–136. <https://doi.org/10.1038/nrm.2016.149>
- Welz, P.S., A. Wullaert, K. Vlantis, V. Kondylis, V. Fernández-Majada, M. Ermolaeva, P. Kirsch, A. Sterner-Kock, G. van Loo, and M. Pasparakis. 2011. FADD prevents RIP3-mediated epithelial cell necrosis and chronic intestinal inflammation. *Nature*. 477:330–334. <https://doi.org/10.1038/nature10273>
- Yang, D., Y. Liang, S. Zhao, Y. Ding, Q. Zhuang, Q. Shi, T. Ai, S.Q. Wu, and J. Han. 2020. ZBP1 mediates interferon-induced necroptosis. *Cell. Mol. Immunol.* 17:356–368. <https://doi.org/10.1038/s41423-019-0237-x>
- Zhang, T., C. Yin, D.F. Boyd, G. Quarato, J.P. Ingram, M. Shubina, K.B. Ragan, T. Ishizuka, J.C. Crawford, B. Tummers, et al. 2020. Influenza Virus Z-RNAs Induce ZBP1-Mediated Necroptosis. *Cell*. 180:1115–1129.e13. <https://doi.org/10.1016/j.cell.2020.02.050>
- Zinngrebe, J., E. Rieser, L. Taraborrelli, N. Peltzer, T. Hartwig, H. Ren, I. Kovács, C. Endres, P. Draber, M. Darding, et al. 2016. --LUBAC deficiency perturbs TLR3 signaling to cause immunodeficiency and autoinflammation. *J. Exp. Med.* 213:2671–2689. <https://doi.org/10.1084/jem.20160041>

Supplemental material

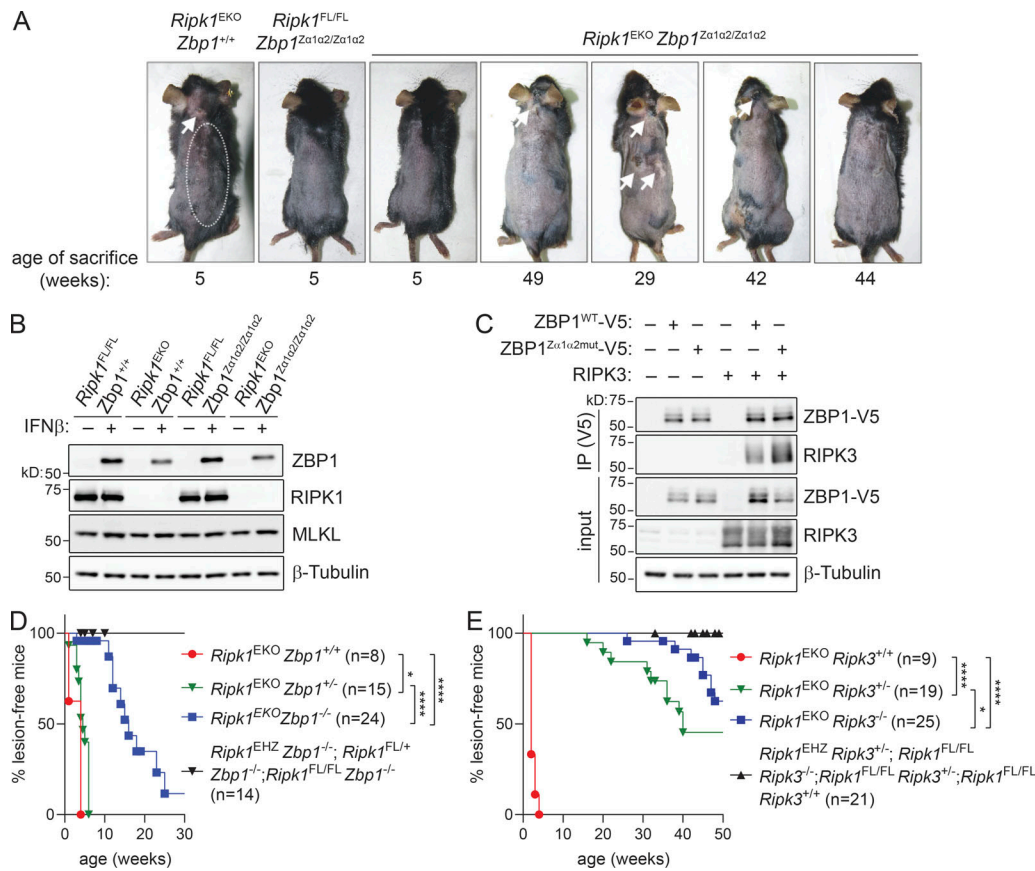


Figure S1. **Skin pathology of *Ripk1^{EKO}* mice is dependent on ZBP1 and RIPK3.** (A) Macroscopic appearance of shaven mice of the indicated genotypes at the indicated age. Lesional skin is depicted by white arrows or by the dotted line. (B) Protein expression analysis by Western blotting on lysates of primary keratinocytes isolated from mice of the indicated genotypes. Cells were stimulated for 24 h with 200 U/ml IFNβ to induce ZBP1 expression. (C) N-terminally V5-tagged wild-type mouse ZBP1 (ZBP1^{WT-V5}) or Zα-domain mutant ZBP1 (ZBP1^{Zα1α2mut-V5}) and mouse RIPK3 were expressed in HEK293T cells. 24 h later, the presence of ZBP1 and RIPK3 in V5-immunoprecipitates (IP) were analyzed by Western blotting. Protein expression in input samples is shown in the lower panels. (D and E) Kaplan–Meier plots of lesion appearance of *Ripk1^{EKO}* mice crossed to (D) ZBP1-deficient (*Zbp1^{-/-}*) or (E) RIPK3-deficient (*Ripk3^{-/-}*) animals. *, P < 0.05, ****, P < 0.0001 by log-rank test. Data shown in B and C are representative of at least two independent experiments.

Downloaded from https://rupress.org/jem/article-pdf/127/17/e20191913.pdf by Universiteit Gent user on 11 May 2020

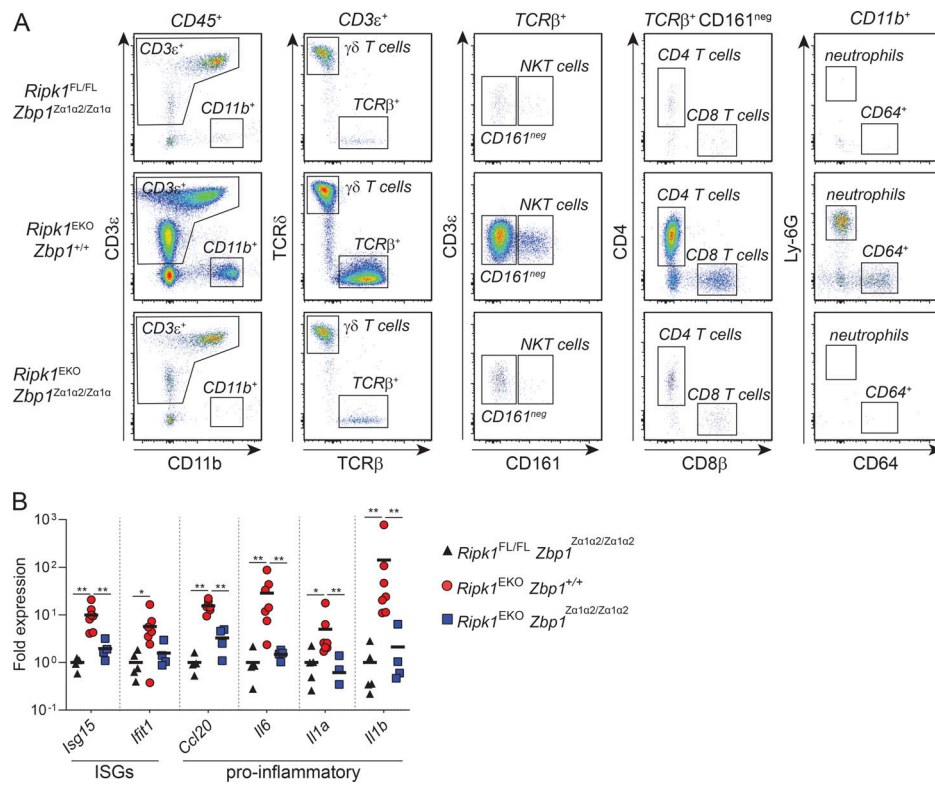


Figure S2. **ZBP1 activation drives antiviral and IL-17 immune responses in *Ripk1^{EKO}* mice.** (A) Flow cytometry gating strategy of CD45⁺ immune cell subsets isolated from mice of the indicated genotypes and quantified in Fig. 2 A. (B) RT-qPCR analysis of the indicated ISGs and pro-inflammatory genes in whole back skin of 4–5-wk-old mice of the indicated genotypes. Data are representative of two independent experiments. *, P < 0.05, **, P < 0.01 by Mann–Whitney U test.

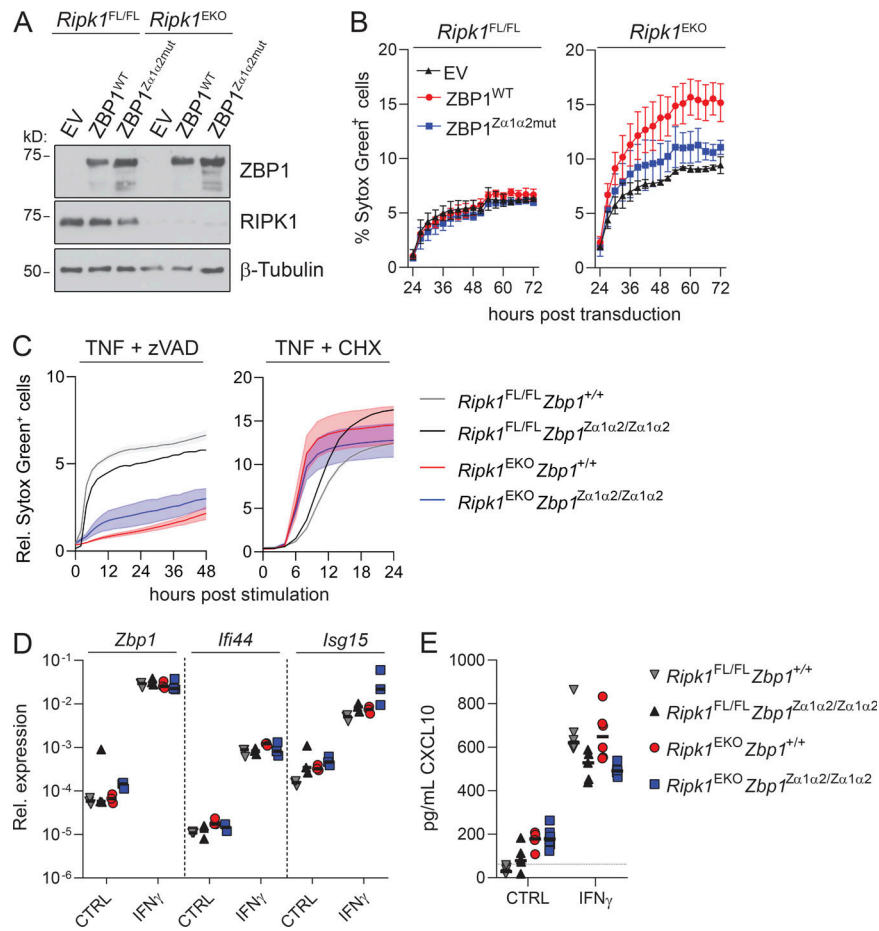


Figure S3. ZBP1 activation by endogenous nucleic acids induces necroptosis in RIPK1-deficient keratinocytes. (A) Primary keratinocytes isolated from the indicated genotypes were transduced with empty vector (EV), wild-type mouse ZBP1 (ZBP1^{WT}) or ZBP1 in which the two Zα-domains were mutated (ZBP1^{Zα1α2mut}). 48 h after transduction, protein expression of ZBP1 and RIPK1 was analyzed by Western blotting. ZBP1 was N-terminally fused to a 3XFLAG and V5-tag. (B) Analysis of cell death by measuring Sytox Green uptake on primary keratinocytes, transduced as described in A. Measurements were performed every 3 h starting at 24 h until 72 h after transduction. (C) Analysis of cell death upon stimulation with 30 ng/ml TNF with 20 μM zVAD-fmk (T + z) or 30 ng/ml TNF with 5 μg/ml CHX (T + C) by measuring Sytox Green uptake every 2 h of primary keratinocytes isolated from mice of the indicated genotype. Solid lines represent the mean of cell death curves of one to four primary keratinocyte cultures isolated from different mice. Shaded areas indicate SEM. (D) RT-qPCR analysis of the indicated ISGs after 18 h stimulation with 200 U/ml IFN γ of primary keratinocytes isolated from mice of the indicated genotypes. (E) Measurement of CXCL10 protein levels in supernatant collected from cells from D by ELISA. The dotted line indicates the detection limit. Data in A–E are representative of two independent experiments.

Downloaded from https://rupress.org/jem/article-pdf/121/7/1620/191913/1042925/jem_20191913.pdf by Universiteit Gent user on 11 May 2020